Magnetic-field and quantum confinement asymmetry effects on excitons

P. Pereyra*
Department of Physics and Astronomy and Condensed Matter and Surface Sciences Program, Ohio University, Athens, Ohio 45701–2979
and Departamento de Ciencias Básicas, Universidad Autónoma Metropolitana-Azcapotzalco, Av. S. Pablo180, C.P. 02200, México D.F., Mexico

S. E. Ulloa
Department of Physics and Astronomy and Condensed Matter and Surface Sciences Program, Ohio University, Athens, Ohio 45701–2979

(Received 5 October 1998; revised manuscript received 29 June 1999)

A theoretical analysis and calculation of the excitonic states in asymmetric quantum dots is carried out in the presence of magnetic fields. The lack of rotational symmetry, introduced by strains and structural factors, produces splittings of the excitonic states with corresponding consequences on the optical oscillator strengths and polarization dependence. For example, we find that the asymmetry produces Zeeman splittings that are smaller than those for symmetric dots at small fields, which could be used as an additional diagnostic of the geometry of the structure. We focus our calculations on naturally occurring quantum dots due to layer fluctuations in narrow quantum wells. Moreover, we observe that increasing magnetic fields produce an interesting crossover to pure angular momentum states for all the excitonic eigenstates, regardless of the degree of asymmetry of the dots and their size. Explicit calculations of photoluminescence excitation yields are presented and related to the different degrees of freedom of the system.

I. INTRODUCTION

To study one of the most significant and defining features of quantum dots, the discrete character of its energy spectrum, a number of photo- and magneto-luminescence (as well as capacitance) experiments have been performed on a variety of systems of quantum dots. The recent development of high spatial and spectral resolution photoluminescence methods have contributed greatly to unveil single-quantum-dot spectral features. As a result, the typical inhomogeneous and broad photoluminescence (PL) structures seen in large assemblies of dots[1–6] split into series of sharp peaks when imaged with increasing resolution, providing important insights of the single-quantum-dot excitonic spectra. Among these beautiful studies of PL and PL excitation (PLE) spectra under external magnetic fields, and for different polarization geometries, we mention those of Refs. 7–13. Even though previous theoretical work provides important information on the exciton properties in a single quantum dot, some questions still remain. The purpose of the present work is to deepen the understanding of the exciton characteristics in symmetric and asymmetric quantum dots in a magnetic field and to account for recent experimental results, where fine structure splittings consistent with characteristic asymmetry interface fluctuations are suggested.[11]

The ground-state properties of confined excitons in quantum dots have been studied by variational and configuration-interaction methods,[14–16] numerical matrix diagonalization schemes,[16–18] or other numerical methods which directly solve the relevant differential equations.[19–21] Some features related to excitons in quantum dots, such as the various exciton states, their degeneracies and level spacings, as well as the diamagnetic shifts, Zeeman splittings, and photoluminescence spectra, have been shown to depend strongly on the interplay of the quantum-dot size and the Coulomb and the magnetic interactions. These and other physical properties are to be addressed in this paper in a unified approach for symmetric and asymmetric quantum dots. Although our numerical results are obtained using typical parameters for quantum dots formed by thickness fluctuations in narrow $Al_xGa_{1-x}As/GaAs$ quantum-well structures, similar qualitative features are expected in all quantum-dot structures, after proper scaling of the physical quantities is made, as discussed further below.

Varying the effective geometrical confinement features (related to the quantum-dot size and asymmetry) and the magnetic field, we explore the degree of influence of the various characteristic length scales in the problem. The magnetic length $l_B=\sqrt{\hbar c/eB}$; the characteristic lateral extension of the dot, L, and the effective Bohr radius for the exciton, $a_B^*=\hbar^2\varepsilon/\mu e^2$, compete with one another. Here ε is the dielectric constant of the medium, and μ is the reduced mass of the exciton. For fixed quantum well widths L_z (or dot heights, see Fig. 1) and a given quantum-dot lateral asymmetry $\eta=L_y/L_x$, different physical regimes correspond to different ratios between the characteristic length scales. At low magnetic fields and small quantum-dot sizes $L=\sqrt{L_xL_y}$, i.e., in the regime where $l_B \gg L \approx a_B^*$, optical properties associated with excitons localized in these structures reflect clearly the effects of geometric asymmetry (especially for PLE). As an example, it will be shown that by losing rotational symmetry the angular momentum is no longer conserved and then, with no good quantum number any more, the corresponding well-defined values for the ground state collapse. We analyze this effect and show that for increasing magnetic field, the exciton and single-carrier states tend to recover a well-defined angular momentum. The mix-

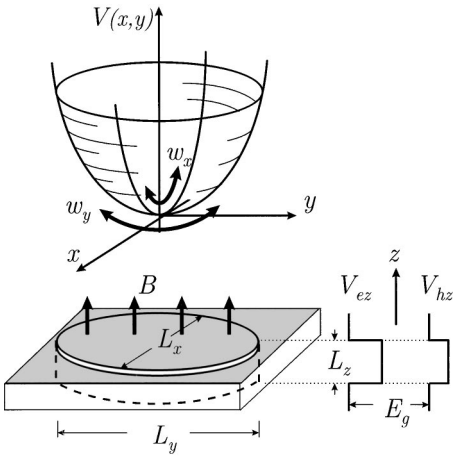

FIG. 1. An asymmetric and flat quantum dot, with height $L_z \ll L = \sqrt{L_x L_y}$, produced as a quantum-well width fluctuation is subjected to an external magnetic field B along the z axis. An e-h pair in the quantum dot is assumed to be confined by a lateral parabolic potential $V(x,y)$, with harmonic oscillator frequencies $w_x \propto 1/L_x^2$ and $w_y \propto 1/L_y^2$. The conduction and valence band-edge potential energies V_{ez} and V_{hz} are shown, respectively, for electrons and holes in the quantum well of width L_z.

ing of well-defined angular momentum states induced by non-symmetric boundaries are weakened by strong magnetic confinement, as one would intuitively expect. As the lateral confining potential gets stronger (due to narrow and/or deeper lateral confining or stronger magnetic fields) the Coulomb interaction is relatively less important, in agreement with recent experiments.[4] It is clear, however, that for certain regions of parameter space, the electron-hole (e-h) interaction becomes significant and even dominant. This is the case, certainly, for quantum dots larger than the mean e-h size ($L \gg a_B^*$, where the geometrical confinement and asymmetries play no significant role). This work analyzes the interplay of all these factors in terms of exciton binding energies and the general characteristics of low-lying excited states of excitons, their e-h separation, angular momentum, and contribution to the optical susceptibility for symmetric and asymmetric quantum dots in the presence of an external magnetic field. Figures 2 and 3 (as well as Fig. 10), shown below, represent typical examples of our most important results in a most succinct form, which is further directly comparable with experiments. This paper will then be devoted to explore the origin as well as the magnetic field and parametric behavior of the different spectral features seen in possible PL and PLE experiments.

In the following two sections, we will describe the model and the procedures used to obtain important excitonic characteristics, including the optical response. We discuss there the physical implications and limitations of the model. In Sec. IV we present sample results and study the excitonic behavior for various structural parameters and magnetic fields. Section V summarizes our conclusions.

II. EXCITONS IN PARABOLIC CONFINEMENT AND MAGNETIC FIELD

The carrier confining potential in a quantum dot depends substantially on the particular method used to create this system. For quantum dots created by layer fluctuations in narrow quantum wells, it is safe to assume that the lateral confining potential is much weaker than the confinement produced by the quantum well potential. Therefore, one can reliably neglect the heavy- and light-hole mixing[22] and consider also the approximation where the lateral motion is decoupled from the z-axis degree of freedom. At low excitation power experiments, less than one e-h pair per quantum dot is excited, on the average. It is thus appropriate to study the physics of one exciton in a quantum dot when additional confinement is produced by applying tunable external magnetic fields. This system is described by the Schrödinger equation with a Hamiltonian given by

$$H = H_e + H_h + H_{e\text{-}h}. \tag{1}$$

Here,

$$H_i = \frac{(\mathbf{p}_i \pm e\mathbf{A}_i/c)^2}{2m_i} + \frac{1}{2} m_i (w_x^2 x_i^2 + w_y^2 y_i^2) + V_{iz}, \quad i = e,h \tag{2}$$

where V_{iz} is the quantum-well confinement potential and

$$H_{e\text{-}h} = -\frac{e^2}{\varepsilon |\mathbf{r}_h - \mathbf{r}_e|}. \tag{3}$$

The in-plane anisotropic harmonic confinement ($w_x \neq w_y$, in general) is understood to be the result of actual structural/geometrical constraints in addition to strain fields present in the system. The latter are especially important in the case of self-assembled dots[1–3] and in strain-defined structures.[4] Notice that this Hamiltonian cannot completely be decoupled, neither in the lateral and z-axis motion nor in the center of mass and relative coordinates. The strategy will be as follows. We shall first make an approximate decoupling between the z and x-y coordinates. To deal with the Hamiltonian in the x-y plane, we will transform to the set of center of mass and relative coordinates. Corrections to these approximations can be implemented systematically, as we will discuss below.

In the effective mass approximation for quantum wells, the hole subbands are treated independently, and each subband is characterized by a pair of effective masses $m_\perp$ and $m_\parallel$, perpendicular and parallel to the quantum well, i.e., *along* and across the growth direction z. It is known that these masses, in terms of the Luttinger parameters, are $m_{h\parallel} = \gamma_1 - 2\gamma_2$ and $m_{h\perp} = \gamma_1 + \gamma_2$.[23] For numerical calculations one can take specific effective masses, such as those for $Al_{0.3}Ga_{0.7}As/GaAs$, with corresponding dielectric constant ($\varepsilon = 13.1$ in GaAs), as we have in mind the quantum-well system reported in Ref. 11. However, other material systems can be equally treated. Much of the physical discussion can be immediately applied after proper scaling has been made by the effective Bohr radius of the problem, a_B^*.

To decouple the z-axis motion from the x-y plane motion we rewrite the Coulomb interaction as

$$H_{e\text{-}h} = -\frac{e^2}{\varepsilon r_{xy}} + \frac{e^2}{\varepsilon}\left(\frac{1}{r_{xy}} - \frac{1}{|\mathbf{r}_e - \mathbf{r}_h|}\right) = -\frac{e^2}{\varepsilon r_{xy}} + \Delta H_{e\text{-}h} \tag{4}$$

and treat $\Delta H_{e\text{-}h}$ as a small perturbation, as discussed in detail elsewhere.[24] Notice that the effective expansion parameter is proportional to the ratio of the expectation value of the relative z coordinate to the in-plane extension ($\approx$ Bohr radius), $\langle|z_h-z_e|\rangle/\langle r_{xy}\rangle \lesssim L_z/L$, and since $L_z/L \simeq 0.1$ in the typical systems under study, this is indeed a small perturbation. In this paper we neglect this perturbative contribution.

Since the first excited state in the z direction, E_1^z, is several tens of meV above the ground state E_0^z (for both electrons and holes), we include only the latter in our calculations and reduce the problem to the calculation of the in-plane motion eigenstates with energies E_n^{xy}. To describe the lateral motion, we write the Hamiltonian H_{xy} in the center of mass and relative coordinate system, defined as usual by $\mathbf{r}_{xy}=(x_h,y_h)-(x_e,y_e)$, and $(m_h+m_e)\mathbf{R}_{xy}=m_h(x_h,y_h)+m_e(x_e,y_e)$. Here and below, all the hole masses refer to $m_{h\|}$, for motion parallel to the quantum well, but we drop the label for ease of notation. Similarly, the position vectors refer to the x-y plane, and we omit the subindices xy. As in Ref. 19, we find convenient to use the symmetric gauge

$$\mathbf{A}_e=\frac{1}{2}\mathbf{B}\times(\mathbf{r}_e-\mathbf{r}_h) \text{ and } \mathbf{A}_h=\frac{1}{2}\mathbf{B}\times(\mathbf{r}_h-\mathbf{r}_e). \tag{5}$$

In this gauge, the Hamiltonian H_{xy} takes the form

$$H_{xy}=H_{COM}+H_{rel}+H_c, \tag{6}$$

where

$$H_{COM}=\frac{P^2}{2M}+\frac{M}{2}(w_x^2X^2+w_y^2Y^2), \tag{7}$$

$$H_{rel}=\frac{p^2}{2\mu}+\frac{1}{2}\mu(\tilde{w}_x^2x^2+\tilde{w}_y^2y^2)+\frac{1}{2}\gamma w_{c\mu}l_z-\frac{e^2}{\varepsilon r}, \tag{8}$$

and

$$H_c=-\frac{ie\hbar}{Mc}B\left(x\frac{\partial}{\partial Y}-y\frac{\partial}{\partial X}\right). \tag{9}$$

Although the decoupling is not complete, as evidenced by the presence of H_c, we can say that the center of mass motion is (nearly) in a harmonic potential with the *same* frequencies as the constituent particles, and *independent* of the external magnetic field, as described by H_{COM}. (This B independence is the expected result of having an uncharged center of mass for excitons, unlike the case for like-charge complexes.) H_{rel} describes the relative excitonic motion, which does depend strongly on the magnetic field. As will be shown below, the term H_c which couples the center of mass and the relative-motion degrees of freedom, is a weak perturbation for the parameters of interest. In the previous equations, we have used the customary notations $M=m_e+m_h$, $\mu=m_em_h/M$, and defined $\gamma=(m_h-m_e)/M$, and

$$\tilde{w}_{x(y)}^2=w_{x(y)}^2+w_{c\mu}^2/4, \tag{10}$$

with $w_{c\mu}=eB/\mu c$.

The magnetic-field effects are of two types: those producing the so-called *diamagnetic* shift, associated with the magnetic dependence on the effective parabolic confinement in Eq. (8), as given by $\tilde{w}_x$ and $\tilde{w}_y$; and the orbital *Zeeman* splitting induced by the Hamiltonian term, which depends on the angular momentum l_z. (The *spin* Zeeman splitting is small and will be neglected here.) As mentioned before, we can deal with the rotational symmetry breaking in terms of the asymmetry ratio $\eta=L_y/L_x$ or, equivalently, in terms of the potential curvatures $w_x=\hbar/\mu L_x^2$ and $w_y=\hbar/\mu L_y^2$ (assumed here the same for electrons and holes).

We will find that the contribution of the linear-B term to the energy in Eq. (8), at least for the low-lying energy levels, is rather small over a wide range of magnetic fields. On the other hand, the splittings introduced by this term and the corresponding selection rules would have important consequences in PLE experiments.

III. EXCITON CHARACTERISTICS

To calculate the exciton eigenstates, we use the two-dimensional (2D) harmonic oscillator basis $|n_xn_y\rangle$ for the scaled frequencies $\tilde{w}_x$ and $\tilde{w}_y$ and follow a numerical matrix diagonalization scheme. Taking H_c as a perturbation, we concentrate first on the diagonalization of the separate relative-motion Hamiltonian whose elements are

$$\begin{aligned}\langle n_x'n_y'|H_{rel}|n_xn_y\rangle &= \hbar\tilde{w}_x\left(n_x+\frac{1}{2}\right)+\hbar\tilde{w}_y\left(n_y+\frac{1}{2}\right)-\langle n_x'n_y'|\frac{e^2}{\varepsilon r}|n_xn_y\rangle \\ &+i\frac{1}{4}\gamma\hbar w_{c\mu}\langle n_x'n_y'|(a_x^\dagger a_y^\dagger-a_xa_y)\left(\tilde{\eta}-\frac{1}{\tilde{\eta}}\right)|n_xn_y\rangle \\ &+i\frac{1}{4}\gamma\hbar w_{c\mu}\langle n_x'n_y'|(a_xa_y^\dagger-a_x^\dagger a_y)\left(\tilde{\eta}+\frac{1}{\tilde{\eta}}\right)|n_xn_y\rangle,\end{aligned} \tag{11}$$

with $\tilde{w}_{x(y)}$ as defined above in Eq. (10), the effective asymmetry factor in a magnetic field is $\tilde{\eta}=\sqrt{\tilde{w}_x/\tilde{w}_y}$ [which clearly reduces to $\tilde{\eta}(B=0)=\eta$, and $\tilde{\eta}(B\gg1)\to1$, recovering circular symmetry effectively], and the $a_{x(y)}^\dagger$ operator creates a quantum of excitation at energy $\hbar\tilde{w}_{x(y)}$.

We diagonalize this matrix and obtain the low-lying energy values as functions of the magnetic field, the quantum-dot size, and its asymmetry. For $B=0$, this reduces in the symmetric case to the model discussed in Ref. 17, and more in general to that discussed in Ref. 18. The last two terms in Eq. (11) are responsible for Zeeman splitting and depend on B both through $w_{c\mu}$ and $\tilde{\eta}$, while the latter also depends on the asymmetry of the structure. Notice that for equal particle masses, these terms vanish ($\gamma=0$).

As discussed above, an interesting property to analyze is the competition between the Coulomb interaction and the size quantization. This can be done in terms of the exciton binding energy E_{cb} defined as the difference between the ground-state energies of the problem calculated with and without the Coulomb-interaction term,

$$E_{cb}=\langle\phi_0|H_0|\phi_0\rangle-\langle\Phi_{rel}^0|H_{rel}|\Phi_{rel}^0\rangle. \tag{12}$$

In this equation $H_0=H_{rel}+e^2/\varepsilon r$, and $|\phi_0\rangle$ and $|\Phi_{rel}^0\rangle$ are the ground eigenstates of H_0 and H_{rel}, respectively.

In the strong size-quantization regime, $L \ll a_B^*$, the binding energy at zero and small fields, $E_{cb}(B \approx 0)$, depends strongly on the quantum-dot sizes and is larger for smaller dots. Notice, however, that the Coulomb interaction is a small perturbation to the confinement energy term in this limit. On the other hand, in the Coulomb regime, for $a_B^* \ll L$ (corresponding to dot sizes larger than $\simeq 20$ nm in GaAs, for example), the zero-field binding energy $E_{cb}(B \approx 0)$ becomes independent of the quantum-dot size. The boundary effect in the quantum dot is now a weak perturbation in this case, and the exciton behaves nearly as if it would not feel the boundary. These two extreme regimes provide the framework to understand the behavior of excitons for all intermediate sizes, where both the Coulomb interactions and the confinement energy are comparable in magnitude.

Since the magnetic field enhances the *e-h* pair confinement through the effective $\tilde{w}$ frequencies, it is clear that the Coulomb and magnetic effects in the Hamiltonian would compete with each other as the field and/or size changes. The quantum-dot sizes at which E_{cb} becomes size independent are smaller for $B \neq 0$ than for $B = 0$. In the limit of strong magnetic fields, the binding energy varies linearly with B, as the system passes to the magnetic regime when $l_B \ll L$, and the magnetic confinement is dominant over the structural or geometrical potential. Increasing B effectively reduces the dot size. It is interesting to notice that as the quantum-dot size increases, the center of mass (COM) energy and its associated quantum of energy $\hbar w$ become smaller, and a number of low-lying exciton states corresponding to excitations of the COM motion appear between the ground state and the first relative-motion excited state. This effect is clearly seen in the susceptibility calculations and can also possibly explain equidistant peaks in photoluminescence experiments observed by Kash *et al.*,[25] and by Lipsanen *et al.*[26] We will illustrate this behavior further below with a few sample results.

Having the eigenvectors $|\Phi\rangle = \Sigma_{n_x n_y} c_{n_x n_y} |n_x n_y\rangle$, where the coefficients $c_{n_x n_y}$ are the result of the diagonalization of H_{rel}, it is interesting to calculate other quantities of physical significance and experimental relevance to this problem. Among these, and closely related to the different size regimes, is the mean electron-hole separation for each state,

$$r_{exc} = (\langle r_{e\text{-}h}^2 \rangle)^{1/2} = \left[\sum_{j=x,y} \frac{\hbar}{2\mu \tilde{w}_j} \langle \Phi | (a_j^\dagger a_j^\dagger + a_j a_j + a_j a_j^\dagger + a_j^\dagger a_j) | \Phi \rangle \right]^{1/2}. \tag{13}$$

The value of r_{exc} gives one idea of the binding of the electron and hole and the effective exciton size.

In order to illustrate the effects of magnetic field and size confinement competition, we calculate a quantity very sensitive to rotational symmetry breaking, which is the expectation value of the z component of the angular momentum,

$$\langle l_z \rangle = \frac{i\hbar}{2} \langle \Phi | \left[(a_x^\dagger a_y^\dagger - a_x a_y) \left(\tilde{\eta} - \frac{1}{\tilde{\eta}} \right) + (a_x a_y^\dagger - a_x^\dagger a_y) \left(\tilde{\eta} + \frac{1}{\tilde{\eta}} \right) \right] | \Phi \rangle. \tag{14}$$

The calculation of this quantity is useful to assign angular momentum values and identify angular momentum transitions. Although the angular momentum is strictly not a good quantum number when the rotational symmetry is broken, our angular momentum calculations show that as one reaches the magnetic regime, the exciton states become close to pure angular momentum states, in essence restoring rotational symmetry to the system.

For a direct comparison with recent high spatial and energy resolution experiments reporting well-defined photo- and magneto-luminescence peaks for single quantum dots, we calculate the excitonic contributions to the optical susceptibility of the system,

$$\chi(w) = \sum_l |\langle 0|P|1\rangle_l|^2 (\hbar w - E_l - i\hbar\Gamma)^{-1}, \tag{15}$$

where $\langle 0|P|1\rangle_l$ is the dipole matrix element between the one *e-h* pair in the excitonic state l and the vacuum.[18] E_l is the *total* energy, i.e., the gap energy E_g plus the center of mass and the z-motion component, as well as the relative motion energy in the l state. Physically, $\chi(w)$ describes the possible radiative transitions or exciton recombination or creation processes, whose strengths are determined by the dipole matrix elements. A phenomenological Lorentzian weight factor of width Γ is assumed. This width mimics the finite spectral lifetimes and possible instrument resolution of PL and PLE experiments. One should note that the transition selection rules obtained in the presence of magnetic field are formally quite similar to the $B = 0$ results,[18] since they are also expressed by

$$|\langle 0|P|1\rangle_l|^2 = |p_{cv}|^2 |\Phi_{rel}(\mathbf{r}=0)|^2 \left| \int \Psi_{COM}(\mathbf{R}) d^2\mathbf{R} \right|^2, \tag{16}$$

where p_{cv} is the interband matrix element near the Γ ($k = 0$) point in these cubic materials, and explicit analytical expressions for the other factors are obtainable in a straightforward way.[18] These factors give no exact suppression of transitions in the relative coordinate (or ''hard'' selection rules), but do impose the restriction that COM states accessible via PLE should have even parity (i.e., with both COM harmonic oscillator indexes N_X and N_Y even).

Finally, we will present the results of perturbation theory to explore the contribution of the coordinate coupling term H_c. In this case, the full basis of eigenstates of the system is given by the composition of eigenvectors of the relative motion, $|\Phi_{rel}^k\rangle$, with energy E_{rel}^k, and the COM vectors $|N_x N_y\rangle$, with associated energies $\hbar w_x (N_x + 1/2) + \hbar w_y (N_y + 1/2)$. For convenience in notation, we will denote these states as $|kN\rangle$. From the form of the H_c term, proportional to the COM momentum components, and given that the COM states have definite parity along each direction, one can easily see that the first order in perturbation theory vanishes, $\langle kN|H_c|kN\rangle = 0$, for any set of quantum numbers. Therefore, the first non-vanishing energy correction for a given state E_{kN}^0 (where N is again a shorthand notation for N_X and N_Y) is given by (for the *non-symmetric* dot case)

$$\Delta E_{kN}^{(2)} = \sum_{k'N' \neq kN} \frac{|\langle k'N'|H_c|kN\rangle|^2}{E_{kN}^0 - E_{k'N'}^0} \tag{17}$$

and is then proportional to B^2. Consequently, for moderate values of the magnetic field, as we will see, this effect is small, proving that our decoupling scheme is indeed amply justified.

IV. RESULTS

In this section we present characteristic numerical values for the quantities described in the last section. To be specific, we consider a quantum dot existing in an $Al_{0.3}Ga_{0.7}As/GaAs$ quantum-well structure such as those in Ref. 11, with $\varepsilon = 13.1$ and the various effective masses mentioned in Ref. 27. We also consider a narrow well of 3.1 nm width and the corresponding gap energies. In a simple square well model with finite depth (taking into consideration corresponding band offsets of 240 and 160 meV in the conduction and valence band, respectively), one easily obtains the z-motion contributions to the energy as $E_0^{ez} \simeq 145$ meV and $E_0^{hz} \simeq 38$ meV. The specific values of E_0^{ez} and E_0^{hz} are very sensitive to the input parameters. Since their value, together with the band-gap energy, defines to a great extent the position of the lowest energy PL/PLE peak, these experiments give information not only on the qualitative behavior of the energy levels with the magnetic field, but are also useful to determine directly important input parameters related to the quantum-well effective sizes.[23]

To calculate the eigenenergies and eigenstates of the relative motion, we construct complex matrices of dimension up to 484×484 for the relative-motion Hamiltonian in Eq. (8). It was shown before,[18] that the dimension of the basis set used has to be larger for larger dots, as more and more states are mixed by the Coulomb interaction. The convergence is in fact rather slow for dot sizes larger than $\simeq 25$ nm, and the matrix sizes required then are at the maximum considered here. We should comment that the model of infinite harmonic confinement is not entirely valid for $L \lesssim L_z$, since it ignores leaking of the wave function into the surrounding medium which is likely for small sizes.

As mentioned earlier, Figs. 2 and 3 present samples of our most representative results for symmetric dots. They summarize all the physical information of the excitonic states and their consequent ''oscillator strength,'' relevant in possible PLE experiments, for example. Figure 2 shows two sets of prominent peaks indicated by arrows, both of which arise from the relative-motion ground state of the exciton in this circularly symmetric ($\eta = 1$) dot. The lower set, here at about 1760 meV at $B = 0$, comes from the zero-point motion of the COM, while the higher set (at $\simeq 1860$ meV) includes one quantum of the COM and is then a ''replica'' of the first set. [The replica appears at $2\hbar\tilde{w} = 102$ meV here, since only $(N_X, N_Y) = (0,0)$, for lower set, and (0,2) or (2,0), for the higher set, are optically accessible, according to the ''selection rules'' discussed above.] The relatively weak magnetic field dependence of these two peaks, blue-shifting by $\simeq 10$ meV for 27 T, is the diamagnetic shift of the relative-motion ground state via $\tilde{w}$, and made here rather small given the strong confinement of the 6 nm dot. The other peaks in this

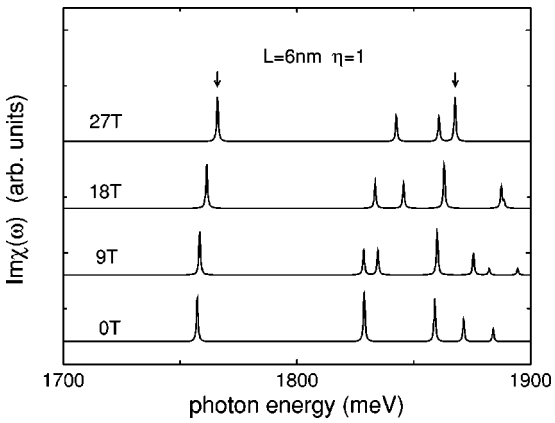

FIG. 2. Optical susceptibility from excitons for a symmetric quantum dot ($\eta = 1$) 6 nm in size, for several magnetic field values. Arrows point to center of mass replicas of the ground state of the exciton. Other peaks are excited states of the exciton. Here, $\hbar w_x = \hbar w_y = 51$ meV.

figure are excitations of the exciton's relative coordinate and show a strong orbital Zeeman splitting (see peaks between the two arrows, in particular) in addition to the diamagnetic shift. The characteristic ''small dot'' spectrum would then exhibit strong Zeeman splittings of the low-lying states, as shown here. Since the COM replicas appear at higher energies, they would possibly not be seen in experiments. Such Zeeman splitting behavior has been well described by Rinaldi *et al.*[4] (although ignoring excitonic effects) and by Wilson *et al.*[6]

In Fig. 3, on the other hand, we show typical results for a much larger symmetric ($\eta = 1$) dot with 14 nm in lateral size. Here, the COM replicas appear much closer together, since $2\hbar\tilde{w} = 18.7$ meV. Moreover, the replicas appear even closer than excited states of the excitonic relative coordinate, which only come after the first replica for $B = 0$, and having a strong magnetic dependence, quickly shift to beyond the second replica for $B > 10$ T.

From these sample dot ''portraits,'' one can appreciate that exploring the magnetic field dependence of the spectral features is extremely important in their proper assignment. It is also clear that detailed analysis of this dependence yields

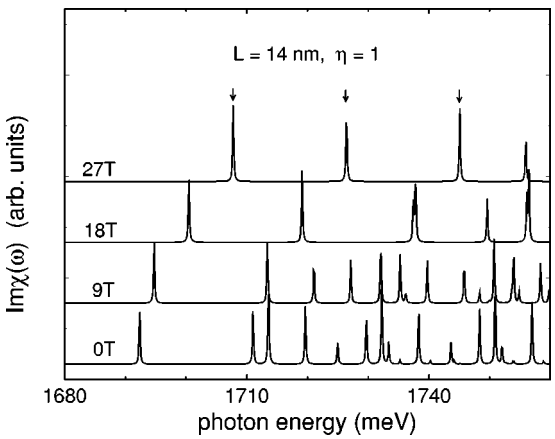

FIG. 3. Optical susceptibility for a larger circular dot, $L = 14$ nm. Notice excited exciton states appear *after* the first center of mass replica (shown by arrows). Here, $\hbar w_x = \hbar w_y = 9.4$ meV.

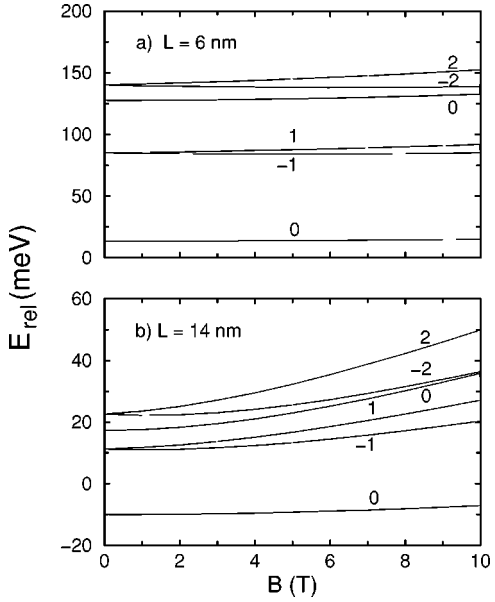

FIG. 4. Six lowest-energy states of the exciton relative-coordinate component, E_{rel}. Labels indicate the quantized value of $\langle l_z \rangle/\hbar$ of each state in these circular dots ($\eta=1$) with different sizes.

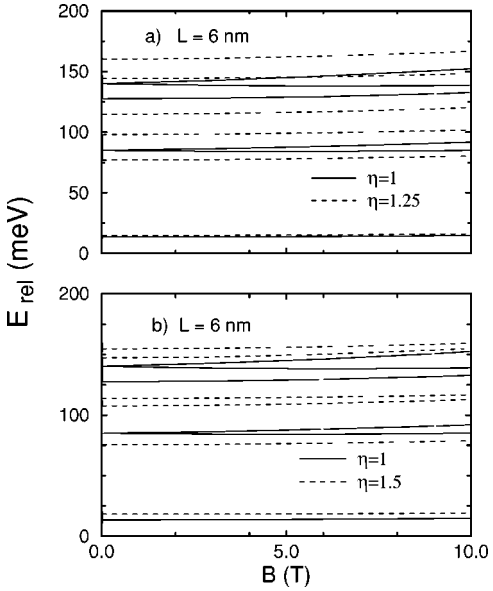

FIG. 5. Relative-motion eigenstates for different asymmetry values and $L=6$ nm. Solid lines are results for the circular dot. Notice how larger η in (b) yields larger splittings. For any $\eta \neq 1$, the zero-field degeneracies are lost.

also insights into the structural or geometrical features of the dots, as we explain from our analysis below.

Since the center of mass motion has no magnetic field dependence, the entire magnetic field evolution of the exciton level structure comes from $H_{\rm rel}$. Figure 4 shows typical results for symmetric quantum dots with sizes $L=6$ and 14 nm for the low-lying relative-motion exciton states. The states are each labeled with the corresponding value of the angular momentum l_z, a good quantum number in these symmetric ($\eta=1$) cases. The level arrangement, Zeeman splitting, and overall magnetic-field dependence is clearly reminiscent of atomic levels, with the added diamagnetic shift via $\tilde{w}$ being more important for larger dots. One important feature, mentioned frequently in the literature, is the energy difference between the ground and the first excited states. This difference is clearly proportional to the binding energy, E_{cb}, and is directly measurable in PLE experiments. We see that this quantity decreases as a function of L and is a good indication of the quantum dot size.

In Fig. 5, we show similar evolution for quantum dots with the same small characteristic length $L=\sqrt{L_x L_y}=6$ nm but with different ratios $\eta=L_y/L_x$. To show the asymmetry effects, we plot the low-lying relative-motion energies for symmetric (solid lines) and asymmetric (dotted lines) states. We notice a general blueshift of the ground state, produced by the smaller size of the dot in one direction. This blueshift tends to disappear as the magnetic field increases (although slowly for these parameters), as one would expect the magnetic field to take over in that limit. The asymmetry-induced blueshift effect is much more evident if one considers the total energy, however. This is the case with the luminescence, and will be shown there. Notice that the full PLE spectra depend on the center of mass energies which depend on the asymmetry ratio η through a factor which grows almost linearly with asymmetry.[28] More importantly, however, the asymmetry breaks the level degeneracies at $B=0$, as clearly shown in Fig. 5. These splits are even rather dramatic for the second and third excited states, for increasing η, and would be quite evident in PLE experiments.

The binding energies E_{cb} have been plotted in Fig. 6, for different quantum-dot sizes and different asymmetry ratios η. The upper three curves correspond to $L=6$ nm, with $\eta=L_y/L_x=1,1.5$, and 2. It is clear from these three curves that one of the effects of asymmetry is to lower the binding energy at $B=0$, with respect to the symmetric case, as the dot getting larger in one direction seems to dominate. The second set of three curves is for $L=18$ nm. Notice that already at this size, the binding energy is somewhat close to its asymptotic (size independent, as for large dots) value, which depends only on the magnetic field. For a given magnetic field, the binding energy is closer to its asymptotic value for quantum-dot diameters beyond certain L_m, which depends on the magnetic field. For $B=0$, this regime is reached for $L_m \sim 30$ nm, while for $B=27$ T, it is reached when $L_m \sim 15$

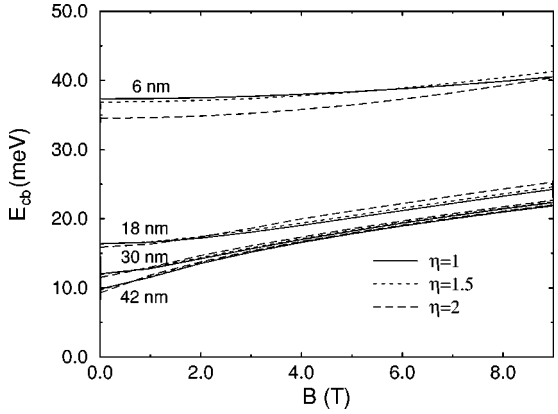

FIG. 6. Exciton binding energy as a function of magnetic field for various dot sizes and asymmetries. For larger dots, the binding energy increases almost linearly with the field over this range.

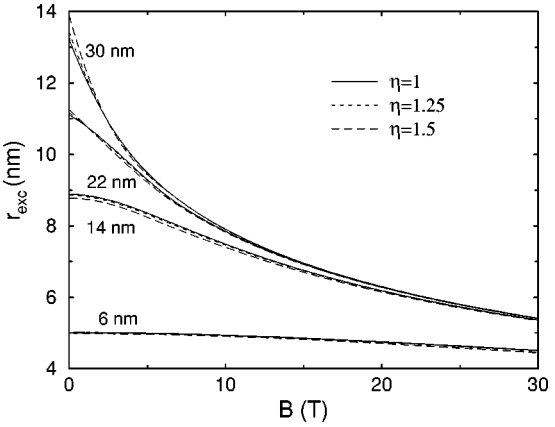

FIG. 7. Exciton ''size'' for the ground state and different dot sizes and asymmetries. As field increases, the effective exciton size decreases, as the magnetic length takes over the confinement.

nm. At the same time, given the rather strong magnetic fields, the asymmetry effects disappear, and the binding energy depends mostly on B, as l_B controls the effective confinement geometry. Correspondingly, the behavior of the exciton ''size'' in the ground state as a function of the magnetic field shows a fast drop as B increases, especially for larger dots (see Fig. 7). It is clear, but surprising, that moderate asymmetries do not influence strongly either E_{cb} or r_{exc}, as they represent perhaps quantities that average over the entire dot domain.

On the other hand, we have seen that excited states of the relative coordinates show clear Zeeman splittings, in addition to the diamagnetic shifts, and one can explore the effects of dot asymmetries on these quantities. Figure 8 illustrates such effect, by showing the first pair of excited states (E^+ and E^-) as functions of the magnetic field, for symmetric ($\eta=1$, SYM) and asymmetric ($\eta=1.25$, ASYM) quantum

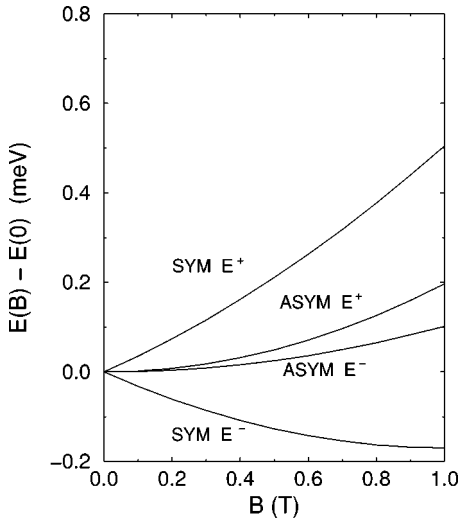

FIG. 8. Illustration of the orbital Zeeman level splitting for a symmetric (SYM, $\eta=1$) and asymmetric (ASYM, $\eta=1.25$) quantum dot with $L=18$ nm. Shown here are the lowest two excited states of the exciton, shifted by the zero-field values, $E^+(B)-E^+(0)$ and $E^-(B)-E^-(0)$, to emphasize the B dependence of the Zeeman shift. Notice that the asymmetry strongly suppresses the linear splitting at low field.

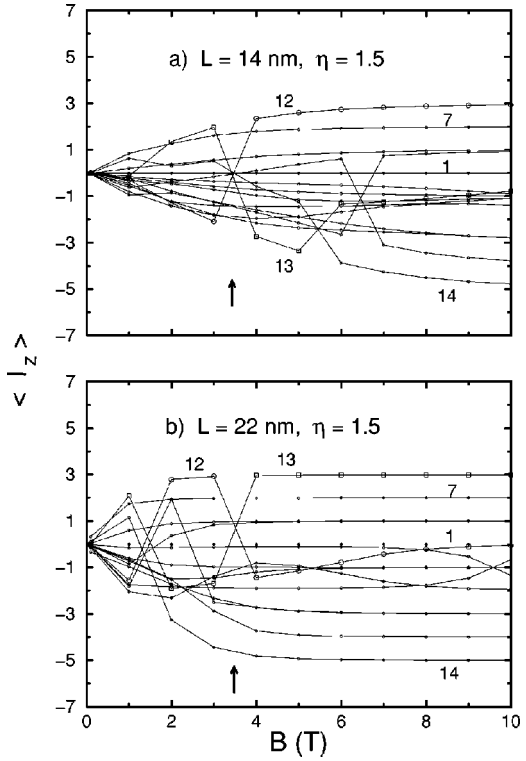

FIG. 9. Expectation values of l_z (in units of $\hbar$) for first 15 relative-motion levels of asymmetric quantum dots. Points are calculated values; solid lines are just guidelines to follow its evolution in each energy level. Notice $\langle l_z\rangle$ evolves continuously in some levels, while in others, it experiences abrupt changes due to energy level crossings. For example, in the ground state (label 1) and the 7th energy level, there are no energy level crossings thus no abrupt changes in $\langle l_z\rangle$. Changes in the 13th energy level appear as it crosses 12th and 14th, as explained in the text. Notice, the strong suppression of $\langle l_z\rangle$ due to asymmetry is lifted for high magnetic fields, and circular symmetry is recovered.

dots with $L=\sqrt{L_xL_y}=18$ nm. These $E^{\pm}$ are the $\langle l_z\rangle=\pm\hbar$ states in Fig. 4(b) for the SYM case (but for a larger L). Notice we have shifted these curves by $E^{\pm}(B=0)$, to emphasize the net B-dependent shift produced. In the SYM case, $E^{\pm}$ split apart linearly from each other (due to the Zeeman term) up to $B\simeq 0.2$ T, commensurate with their well-defined angular momentum—although the splitting is later taken over by diamagnetic effects. However, for $\eta=1.25$, the ASYM levels hardly split at all for small fields, since their effective angular momentum has basically collapsed to zero (as we will show below), and basically only the quadratic diamagnetic shift remains (notice, for example, the lack of negative dispersion of the E^- ASYM branch). This strong suppression of the Zeeman splitting provides then a strong signature of the asymmetry of the dot which is directly accessible spectroscopically and can in principle even be used to quantify η.

To further illustrate the effects of asymmetry on the dot levels, we look at the expectation value of l_z. Although these values are not directly obtainable from experiments, they do affect the PL and PLE oscillator strenghts and help us understand the underlying physics. Figure 9 shows typical examples of $\langle l_z\rangle$ for different relative-coordinate states of the exciton. The points are the calculated values of $\langle l_z\rangle$ and the

solid lines are just guidelines to indicate the angular momentum evolution of the first, the second, an so on, energy level. In general the z component of the angular momentum of the ith energy level changes when it crosses with the $(i+1)$th or the $(i-1)$th energy level. For example, the z component of the angular momenta of the 12th and the 13th energy levels [in Fig. 9(a)] change somewhere between $B \simeq 3$ and 4 T (see the arrow). The crossed lines indicate that the energy levels cross each other and the angular momentum of the 12th energy level passes from about $-2\hbar$ to about $2.5\hbar$, correspondingly, the angular momentum of the 13th energy level experiences the opposite change. The lowest energy level (label 1) has always $\langle l_z \rangle = 0\hbar$. Both panels show that the otherwise quantized l_z values for circularly symmetric dots ($\eta = 1$) are rather strongly affected by the asymmetry, regardless of the dot size or even η value. For $B \sim 0$, we see that $\langle l_z \rangle$ is nearly zero for all levels (first 15) shown, for small L. As L grows, however, the suppression of $\langle l_z \rangle$ weakens and gives rise to finite but not quantized values of the angular momentum. Asymptotically, however, stronger B fields reinstate rotational symmetry to the system and therefore z-component angular momentum conservation, so that in fact, $\langle l_z \rangle$ recovers well-quantized values in this region, regardless of L and η values (of course, smaller L and/or larger η values require stronger fields for this regime to be reached). [One should notice that sudden crossings in this plot are indicative of the B dispersion of the levels, since the negative dispersion forces rearrangements of level orderings (used as the index in the plotting).] Since different η values produce different degree of $\langle l_z \rangle$ suppression (not shown), one can conversely use this feature (measurable in PLE experiments, as explained in and by Fig. 8) to evaluate the degree of asymmetry of the quantum dots. This, together with light-polarization-dependent shifts,[11] would very nicely complement the analysis of geometrical effects on the spectral response of the system. Notice further that as states recover well-defined $\langle l_z \rangle \neq 0$ values, they also decrease their overall oscillator strength. This effect, fully included in the calculation of the PLE figures, give interesting B-dependent line shapes of the PLE data. We would suggest that detailed analysis of such experiments should serve as additional probes of effective confinement geometries.

From these calculations, and as a synthesis of all these effects, we obtain the linear susceptibility spectra defined in Eq. (15), which one can compare with the experimental photo- and magneto-luminescence excitation measurements. Notice, incidentally, that using the parameters mentioned in Ref. 11, we are in qualitative agreement with the experimental values both in photon energy and in the separation for the system discussed in that reference for $L \simeq 18$ nm. In Fig. 10 we present another example of linear susceptibility for a quantum dot with different size and asymmetry factor. In this figure we plot the susceptibility for several values of B as functions of the photon energy, considering a Lorentzian width of the order of the experimental resolution, $\Gamma = 0.1$ meV. Notice the anticipated diamagnetic shift (quadratic up/blue shifting of all peaks with the B field), introduced via the $\tilde{w}_x$ and $\tilde{w}_y$, both functions of the field. One also clearly sees the Zeeman splitting, just as in Figs. 2 and 3 for $\eta = 1$.

Figure 10(b) illustrates the effect of asymmetry, $\eta = 1.5$,

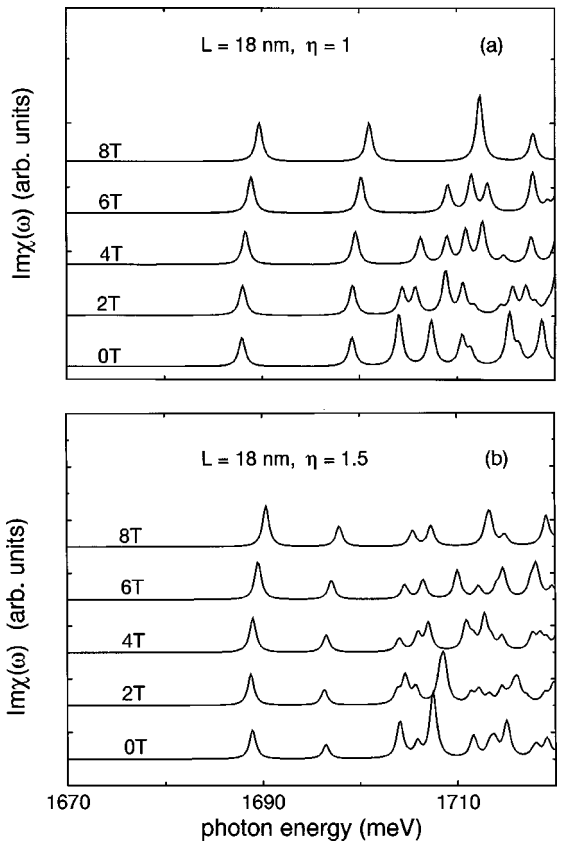

FIG. 10. (a) Exciton contribution to the optical response of a large circular quantum dot, $L = 18$ nm. Arrows indicate the center of mass replicas, as in Figs. 2 and 3. Here, $\hbar\omega_x = \hbar\omega_y = 5.7$ meV. (b) $\eta = 1.5$; notice first center of mass replica is only 7.6 meV from ground state, as $\hbar\omega_y = 3.8$ meV and $\hbar\omega_x = 8.5$ meV.

and the first COM replica moves in closer than in Fig. 10(a), being that $2\hbar w_y$ is only 7.6 meV away from the ground state (at $B = 0$), and the $2\hbar w_x$ replica does not appear until 17 meV from the ground state [the fourth small feature at $B = 0$ in Fig. 10(b)]. (COM replicas are readily identified since they mimic the field dependence of the ground state.) This is of course a reflection of the $(N_X = 2, N_Y = 0)$ and (0,2) splitting produced by the asymmetry of the structure, since $w_y \neq w_x$. Notice, incidentally, that these first replicas appear at half the strength of the ground state (unlike the $\eta = 1$ cases), reflecting the asymmetry splitting once more. The third feature for $B = 0$ is the lowest (degenerate) pair of $\langle l_z \rangle = \pm\hbar$ excited states of the exciton, at $\simeq 15$ meV from the ground state. The (in this case nondegenerate) lowest two excited states of the exciton, split further in the field much more slowly, so that at $B = 2$ T the additional splitting is less than ~ 0.2 meV. This suppressed Zeeman splitting is what we referred to in connection with Fig. 8. Notice that for this set of parameters, the $4\hbar w_y$ replica also contributes to the third feature here (an accidental degeneracy), and explains the enhanced strength at $B = 0$. This replica remains as the third feature at 8 T, while the excited state has shifted to be under the fifth compound peak at that field value. Similarly, the fifth peak at zero field contains several excited-state contributions which split with field, so that the second excited state of the exciton evolves into the rightmost peak at 8 T, while others evolve much faster in field.

Finally, we should comment that we have calculated the lowest nonvanishing order of perturbation theory of the effect of the center of mass and relative motion coupling term H_c, as described in the previous section. Although not shown here, we verify that there is a quadratic field dependence of this term, as discussed before, and the contribution to the lower relative motion energies is negligible. For the lower states, it has nearly no effect on their magnetic-field values, and is found that for $B \lesssim 4$ T, the correction to the energies is $\lesssim 2$ meV. Similarly small shifts result for other L and η values, so that this H_c term provides only a small perturbation, except for the largest of magnetic fields and high COM replicas.

V. CONCLUSIONS

We have explored the magnetic-field dependence of the excitonic levels in asymmetric quantum dots. We have found that, as expected on consideration of the different length scales of the problem, the behavior of these levels depends strongly on the relation among the magnetic length, the Bohr radius of the exciton, and the characteristic size of the dot. For small dots (smaller than approximately 10 nm in GaAs), $L \lesssim a_B^*$, the exciton binding energy is strongly sensitive to the magnetic field, dot size, and asymmetry. As the dot size greatly exceeds a_B^*, the binding energy increases nearly linearly with magnetic field, and is basically independent of dot size or symmetry, as the confinement walls are a small perturbation to the problem.

For asymmetric dots, the lack of angular momentum conservation is reflected in a strong collapse of the expectation value of l_z for nearly all low-lying exciton states, suppressing the orbital Zeeman-like splitting, which is clearly seen in circular dots. This asymmetry is directly observable in the magnetic-field dependence of PLE spectra and should provide a quantifiable probe of the structural features of the luminescent states and dots in which they reside. Analysis of the Zeeman splittings, as well as the weakly B-dispersive center of mass replicas of excitonic states, provide a complete picture of the geometry of the structures.

Although the specific results presented are for a given GaAs-based set of quantum dots created in a narrow quantum well, similar considerations would be valid in general in experiments of other systems, such as self-assembled quantum dots.[1–3,18] There, of course, the confinement is of a three-dimensional nature, but with a level structure produced by a combination of geometrical confinement, strains and dielectric effects. Issues of symmetry of confinement should also play an important role in the observed optical response.

Finally, the role of the symmetry of excitonic states in quantum dots would also give rise to interesting signatures in inelastic scattering of light experiments, for example, such as those performed recently in related systems.[29] Future theoretical work on this issue[24,30] will be presented elsewhere.

ACKNOWLEDGMENTS

We thank C. Trallero-Giner for his suggestion to study this problem, his comments, and careful readings of the manuscript. We also thank A. Govorov for helpful discussions, and J. Song for previous computational work. This has been supported by US Department of Energy Grant No. DE–FG02–91ER45334, and by CONACYT (México) through its Programa de Apoyo para Estancias Sabáticas, Project No. 29026-E, and by the Sabbatical Program from Universidad Autónoma Metropolitana (México).

*Electronic address: ppp@hp9000a1.uam.mx

[1] J.-Y. Marzin, J.-M. Gerard, A. Izrael, D. Barrier, and G. Bastard, Phys. Rev. Lett. **73**, 716 (1994).

[2] R. Leon, P.M. Petroff, D. Leonard, and S. Fafard, Science **267**, 1966 (1995).

[3] M. Grundmann, J. Christen, N. N. Ledentsov, J. Böhrer, D. Bimberg, S. S. Ruvimov, P. Werner, U. Richter, U. Gösele, J. Heydenreich, V. M. Ustinov, A. Yu. Egorov, A. E. Zhukov, P. S. Kop'ev, and Zh. I. Alferov, Phys. Rev. Lett. **74**, 4043 (1995).

[4] R. Rinaldi, P. V. Giugno, R. Cingolani, H. Lipsanen, M. Sopanen, J. Tulkki, and J. Ahopelto, Phys. Rev. Lett. **77**, 342 (1996).

[5] I. E. Itskevich, M. Henini, H. A. Carmona, L. Eaves, P. C. Main, D. K. Maude, and J. C. Portal, Appl. Phys. Lett. **70**, 505 (1997).

[6] L. R. Wilson, D. J. Mowbray, M. S. Skolnick, M. Morifuji, M. J. Steer, I. A. Larkin, and M. Hopkinson, Phys. Rev. B **57**, R2073 (1998).

[7] K. Brunner, U. Bockelmann, G. Abstreiter, M. Walther, G. Böhm, G. Tränkle, and G. Weimann, Phys. Rev. Lett. **69**, 3216 (1992).

[8] A. Zrenner, L. V. Butov, M. Hagn, G. Abstreiter, G. Böhm, and G. Weimann, Phys. Rev. Lett. **72**, 3382 (1994).

[9] K. Brunner, G. Abstreiter, G. Böhm, G. Tränkle, and G. Weimann, Phys. Rev. Lett. **73**, 1138 (1994).

[10] H. F. Hess, E. Betzig, T. D. Harris, L. N. Pfeiffer, and K.W. West, Science **264**, 1740 (1994).

[11] D. Gammon, E. S. Snow, B. V. Shanabrook, D. S. Katzer, and D. Park, Phys. Rev. Lett. **76**, 3005 (1996).

[12] W. Heller and U. Bockelmann, Phys. Rev. B **55**, 4871 (1997).

[13] Y. Toda, S. Shinomori, K. Suzuki, and Y. Arakawa, Appl. Phys. Lett. **73**, 517 (1998).

[14] Al. L. Efros and A. L. Efros, Fiz. Tekh. Poluprovodn. **16**, 1209 (1982) [Sov. Phys. Semicond. **16**, 772 (1982)]; G. W. Bryant, Phys. Rev. B **37**, 8763 (1988); **41**, 1243 (1990).

[15] L. Banyai, Y. Z. Hu, M. Lindberg, and S. W. Koch, Phys. Rev. B **38**, 8142 (1988); T. Takagahara, *ibid.* **39**, 10 206 (1989); S. V. Nair, S. Sinha, and K. C. Rustagi, *ibid.* **35**, 4098 (1987).

[16] Y. Z. Hu, M. Lindberg, and S.W. Koch, Phys. Rev. B **42**, 1713 (1990).

[17] W. Que, Phys. Rev. B **45**, 11 036 (1992).

[18] J. Song and S.E. Ulloa, Phys. Rev. B **52**, 9015 (1995).

[19] V. Halonen, T. Chakraborty, and P. Pietiläinen, Phys. Rev. B **45**, 5980 (1992).

[20] U. Bockelmann, Phys. Rev. B **48**, 17 637 (1993); **50**, 17 271 (1994); U. Bockelmann, Ph. Roussignol, A. Filoramo, W. Heller, G. Abstreiter, K. Brunner, G. Böhm, and G. Weimann, Phys. Rev. Lett. **76**, 3622 (1996).

[21] A. O. Govorov and A. V. Chaplik, Zh. Éksp. Teor. Fiz. **99**, 1853 (1991) [Sov. Phys. JETP **72**, 1037 (1991)].

[22] D. A. Broido and L. J. Sham, Phys. Rev. B **31**, 888 (1985).

[23] P. Y. Yu and M. Cardona, *Fundamentals of Semiconductors* (Springer Verlag, New York, 1996).

[24] E. A. Menendez-Proupin, C. Trallero-Giner, and S. E. Ulloa (unpublished).

[25] K. Kash, D. D. Mahoney, B. P. Van der Gaag, A. S. Gozdz, J. P. Tarbisson, and L. T. Florez, J. Vac. Sci. Technol. B **10**, 2030 (1993).

[26] H. Lipsanen, M. Sopanen, and J. Ahopelto, Phys. Rev. B **51**, 13 868 (1995).

[27] While in the 3 nm GaAs layer we consider $m_{h\|}=0.1m_0=m_{hxy}$, $m_{hz}=0.45m_0$, and $m_e=0.067$, in the $Al_{0.3}Ga_{0.7}As$ layer we have $m_{h\|}=0.13m_0=m_{hxy}$, $m_{hz}=0.54m_0$, and $m_e=0.092m_0$.

[28] In fact, the full expression for the COM energy is $E_{\mathrm{COM}}=\hbar w_x(N_X+\frac{1}{2})+\hbar w_y(N_Y+\frac{1}{2})=(\hbar/\mu L^2)\{N_X/\eta+\eta N_Y+\frac{1}{2}(\eta+\eta^{-1})\}$, which for large η grows almost linearly with it.

[29] D. J. Lockwood, P. Hawrylak, P. D. Wang, C. M. Sotomayor Torres, A. Pinczuk, and B. S. Dennis, Phys. Rev. Lett. **77**, 354 (1996).

[30] P. Pereyra (unpublished).